

DEVELOPMENT OF AN UNDERWATER HIGH
SENSITIVITY CERENKOV DETECTOR: SEA URCHIN

Ugo Camerini

University of Wisconsin, Madison, Wisconsin 53706

Donald McGibney

Hawaii DUMAND Center, University of Hawaii, Honolulu, Hawaii 96822*

Arthur Roberts

Hawaii DUMAND Center, University of Hawaii, Honolulu, Hawaii 96822

Roland Winston

University of Chicago, Chicago, Illinois 60680

ABSTRACT

The need for a high gain, high sensitivity Cerenkov light sensor to be used in a deep underwater muon and neutrino detector (DUMAND) array has led to the design of the SEA URCHIN detector. In this design a spherical photocathode PMT is optically coupled through a glass hemisphere to a large number of glass spines, each of which is filled with a wavelength-shifting (WLS) solution of a high quantum efficiency phosphor. The Cerenkov radiation is absorbed in the spine, isotropically re-radiated at a longer wavelength, and a fraction of the fluorescent light is internally reflected in the spine, and guided to the photomultiplier concentrically located in the glass hemisphere. Experiments measuring the optical characteristics of the spines and computer programs simulating light transformation and detection cross sections are described. Overall optical gains in the range 5-10 are achieved. The WLS solution is inexpensive, and may have other applications.

*On leave from Center for Naval Analyses, Alexandria, VA 22311

1.0 INTRODUCTION

In this paper we describe the design of a high-gain, high-sensitivity Cerenkov detector that we have called Sea Urchin. Sea Urchin was intended to provide a high-sensitivity optical detector module for a deep underwater muon and neutrino detector (DUMAND) array, in which the spacing of the optical detectors depends critically on their sensitivity and where the necessary number of high sensitivity detectors varies inversely as the cube of their spacing for a given array volume.

Although the Sea Urchin detector was designed for underwater detection of the Cerenkov radiation emitted by charged muons and hadronic cascades, the detector as designed may also be used in an atmospheric environment. In air its overall efficiency will approximately double, because of increased collection of the fluorescent light, with an external medium of lower index of refraction. Even though it has proven unsuitable for its original purpose because of its great bulk and weight, and the difficulty of installing it in the ocean, we believe the design may prove useful under less exigent conditions.

1.1 Basic Design.

In Sea Urchin a hemispherical-cathode photomultiplier tube (PMT) is optically coupled to a large number of radial glass "spines", each a transparent tube filled with a wavelength-shifting solution that captures and reradiates the incident Cerenkov light, and transmits a fraction of the re-radiated light to the photomultiplier cathode.

Figure 1 shows the Sea Urchin detector module in its operating configuration. The most favorable design uses 900 eight-foot long one-inch diameter glass spines, each filled with a solution of Hostasol Yellow 8G in toluene, a proprietary fluor* with high efficiency in shifting Cerenkov light centered at about 440 nm to green light at about 510 nm.

2.0 PRINCIPLE OF OPERATION

Figure 2 shows a portion of the Sea Urchin sensor in more detail with only a few of the spines shown. The design that gives the best calculated results uses a 13-inch hemispherical photomultiplier tube (PMT) with the detecting spines affixed radially to a 26-inch diameter glass hemisphere (spherical lens) inside of which the PMT is concentrically located (see Sec. 4.3). The central glass hemisphere is a major component of the design and should be able to sustain the underwater pressure at the depth at which it is to be deployed, so that the spherical lens filling and PMT need not withstand higher than atmospheric pressure. With the indices of refraction of the hemisphere and spine matching (at approximately 1.51) the emerging light cone from the spine will contain over 80% of the light in a half angle cone of about 33 degrees. To avoid reflection at the interfaces, and to collect the emitted light efficiently, the index of refraction should be essentially constant from spine, through the glass hemisphere, fluid coupling medium and PMT glass envelope. The PMT cathode diameter therefore should be close to one-half the glass sphere diameter in order to efficiently intercept the light cone, thus effecting a nearly perfect phase-space match from the PMT to the spines.

*Available from American Hoechst Corp.

Power and detector signals may be transmitted through the sphere either by direct metallic conduction (via conductors in holes) or possibly through the glass. The small power requirement of the module (under 10 watts) makes it possible to use a radio-frequency power source capacitatively coupled through the glass as an alternative to penetrators. Detector signals, too, can be transmitted through the glass by optical means thus avoiding penetrations. Avoiding penetrations in the glass should increase underwater reliability and reduce overall costs.

3.0 EXPERIMENTAL PROCEDURES AND RESULTS

In development of the Sea Urchin concept experimental measurements were carried out on the optical characteristics of the WLS spines; and computer programs were written to simulate the process whereby Cerenkov light is transformed in the spine and collected at the PMT and to determine total Sea Urchin detection cross-section for incident light. In addition experiments were conducted to determine the quantum yield of a selected fluor and the optical efficiency of single spines. Finally, a half-scale model was constructed, assembled and given preliminary tests.

3.1 Spine Design

The most favorable design for a simple cylindrical spine appears to be a thin glass tube, filled with a low-density high index of refraction solvent in which the wavelength shifting fluor is dissolved. Solid or tubular plastic or glass spines with a thin coating of plastic or resin containing the wavelength shifter either on the outside of the rod, as suggested by Viehmann [1], or on the inner surface of the tube, as suggested by Bowen [2], proved less efficient in our tests. A solid transparent plastic with the fluor dissolved in it would be excessively expensive for production of large number of spines. The spine is sealed off with a flat window at the inner end, and provided with a free piston with O-ring seals at the outer end, in order to accommodate the compression of the toluene solvent under the hydrostatic pressure of the ocean.

How are the radiating spines to be supported in optical contact with the glass sphere, and in what sort of matrix must they be embedded? The required properties of the matrix are somewhat contradictory. If it is rigid, it will have to remain permanently in position; it will consist of an overlay with sockets or holes into which the spines will be secured. This alternative would be appropriate for the case where the spines could be assembled as part of the detector module in their final configuration. The spines are relatively fragile, and their weight in air not inconsiderable. They may therefore exert a considerable torque on their mountings and be susceptible to breakage. This objection may be overcome with a permanent supporting framework. Such a system was used in the half-scale model of Sea Urchin.

3.1.1 Flexible Spine Mountings. - - For underwater use, a flexible matrix was developed [3], consisting of a sandwich of foam rubber or similar material between layers of kevlar cloth, which is cut into sectors joined at the center, allowing the entire matrix to be brought into a plane position for introducing the spines into their sockets for transportation. This allowed transport in a configuration requiring much less volume than the final open one. In operation the spines would be opened up like the ribs of an

umbrella, allowing the foam rubber-kevlar cloth sandwich to conform to the spherical surface.

3.1.2 Tests on Optical Properties: Absorption, Emission. - - The apparatus shown in Fig. 3 was constructed to carry out investigations on such variables as optimum spine length and diameter, filling solvent, fluor and fluor concentration. It consisted of a box in which the spine was uniformly illuminated by a light source, filtered to duplicate as closely as possible the Cerenkov spectrum after it has traversed at least one underwater attenuation length. The illumination was made as uniform as conveniently possible by providing four 8-foot fluorescent "daylight" tubes, each covered with theatrical gel "brilliant blue" filters. Figure 4 shows a schematic of the experimental apparatus used to measure the fluorescent emission spectra output of the spine samples. The emission spectrum of the fluorescent spine was measured as a function of wavelength by optically coupling one end of the spine to a lucite light pipe which in turn was coupled to a grating spectrometer. More details are given in Reference 4.

3.1.3 Choice of Fluor. - - The requirements for a suitable fluor are that it have a high quantum yield of fluorescent light; that the absorption spectrum match, as closely as possible, the Cerenkov light spectrum in the ocean; and that the fluorescent light be no redder than necessary to achieve the above objectives. The latter requirement is to ease the difficult problem of finding a photocathode material for detecting the fluorescent light which is highly efficient and not too noisy or too expensive. With the Cerenkov spectrum peaking at about 450 nm, the fluorescent peak will be somewhere around 500 to 540 nm, a region in which the more customary photocathodes exhibit rapidly decreasing efficiency. We imposed the requirement that the fluor be usable with a bi-alkali photocathode, and not require the more expensive tri-alkali S-20.

3.1.4 Choice of Solvent. - - The choice of toluene as solvent was almost inevitable, from the requirements of low cost and high index of refraction, and no absorption in the wavelength range of interest. We have taken extensive data on solutions of fluors in toluene, and ethanol at different concentrations; we have also measured their absorption at the mercury line 438 nm. Some of these data are shown in Fig. 5, plotted as signal intensity vs. wavelength for some of the more active fluors. These high quantum yield fluors include Hostasol 3G and 8G, Acridine Yellow, Rhodamine 6G, Rubrene, and BBQ. Plots are shown only for those fluor concentrations in milligrams per liter which give the greatest fluorescent yield. All curves were taken under identical conditions, so that the responses are directly comparable. The curves are not corrected for the photocathode response of the PMT.

3.2 Measurement of Attenuation of Fluorescent Light.

Integral attenuation curves were obtained by covering all of the spine except the first L centimeters (nearest the PMT), and varying L. Differential curves were obtained by exposing a fixed length of L centimeters along the spine, and varying the position of the exposed region with respect to the detector. Figure 6 shows the differential attenuation plot of Hostasol 8G dissolved in toluene at a single wavelength at the peak of the fluorescent spectrum. The data was taken using a 1/2-inch diameter, 8-foot long spine for four different fluor concentrations as indicated.

Measured attenuation lengths vary from 0.8 meters to 2.1 meters.

In addition to readings taken with the grating spectrometer, it has also been useful to take data in which the spectrometer was replaced by a PMT. In that case the observation measures the quantity that is physically the most significant: the integrated response to the fluorescence spectrum by the PMT. In our case we used a PMT with an Si wide-band response. It is significant that it was in these data that the deviations from a single attenuation length were most marked. Figure 7 is an attenuation curve like that of Fig. 6 for the same fluor, Hostasol Yellow 8G, dissolved in toluene for four different concentrations. These curves, however, represent data taken without the spectrometer. Note the much greater deviation from exponential attenuation, indicating a departure from a single attenuation length when examining the entire spectrum.

3.3 Simulation of Spine Performance.

A Monte Carlo program, called CYL6X, has been developed [4], which simulates and traces in detail the physical process whereby incident Cerenkov light, predominantly in the blue, is transformed in the spine to yellow-green and transmitted by total internal reflection to the PMT photocathode.

In detail, the program assumes that the incident light is uniformly distributed along the spine and averages it over all angles of incidence, weighted by the cosine of the incident angle. At each incident angle the amount of light reflected and transmitted is calculated and the direction of the refracted ray (in the spine) is determined. A coefficient of attenuation of the incident light (ATTINC) is given as data, and the source function for the fluorescent light is found by making it proportional to the primary light absorbed in each element of the track length. The program assumes the fluorescent light to be isotropically emitted with an intensity given by the source function. The propagation down the spine is characterized by a coefficient of attenuation for the fluorescent light (V), and a surface reflection coefficient (SR) that simulates surface imperfections. Light propagating away from the PMT is assumed to be reflected at the end of the spine.

The chief fault in the simulation is the simplification of the incident and fluorescent light interactions with the medium. It is described in each case by a single attenuation coefficient. For the incident light that approximation is good; it amounts to averaging over a range of absorption coefficients rather than using a single fixed value. In the case of the emitted light, however, there are complications. The emitted light spectrum and the incident light spectrum overlap; the effect of this is to make the overlap region disappear quickly, since light emitted in that range is quickly reabsorbed. In addition the self-absorption varies relatively rapidly over the remainder of the spectrum. Thus the mean absorption coefficient is not a constant. Experimentally, a log plot of the differential absorption shows this curvature distinctly (see, e.g., Fig. 7).

Consequently the program is still an approximation; however, it is a sufficiently good one so that it is useful. It enables us to compare and evaluate different situations. The program could be modified to take account of reabsorption and re-emission of light; but this has not been done.

The program was particularly useful in illustrating the importance of various spine parameters. It showed that absorption of the incident light should be high for two reasons: first, to make sure it is all absorbed, and second, because fluorescent light generated near the surface is captured more efficiently than that generated near the axis.

3.3.1 Results. - - Figs. 8A and 8B show the angular distribution of the light emerging from the end of the spine at the PMT, in a medium of the same index of refraction as the spine, as calculated by the CYL6X program. All curves are for a sea-water medium with an index of refraction 1.35, and a spine solvent of index $N=1.56$. In Fig. 8A, curves are plotted for $SR = 0.998$ and 0.990 , with $\alpha \approx 0$. Fig. 8B shows similar curves for $\alpha=0.0016667$. The larger the total attenuation, the more parallel the emergent light.

3.4 Sea Urchin Opacity

The overall effectiveness of the Sea Urchin detector module requires a knowledge of its total cross section for incident light. This is described by a quantity we call "opacity", which is the fraction of the incident light that strikes a spine as it traverses the detector module. Whereas the CYL6X program described above deals with the fate of light that strikes a spine, an opacity program [3] tells us what fraction of the geometric cross-section of the module is effective in intercepting the incident Cerenkov light.

The geometric shape of the array is a hemisphere of radius r . The geometric cross-section in a direction normal to the diametral plane of the hemisphere is πr^2 , and in the direction at right angles that, half as much. The opacity has been calculated in both directions in a Monte Carlo program.

Table 1 is a synopsis of the results of this program. Results were calculated for four module radii of $r = 1, 2, 3$ and 4 meters, three different spine diameters of 1, 1/2, and 1/4 inches, and for three different assumed values of the packing fraction (defined as that fraction of the area of the glass sphere occupied by the spines.) The maximum possible packing fraction for cylindrical spines would be the area of a circle divided by that of the square enclosing it, or $\pi/4 = 0.79$. The effective cross section areas shown in Table 1 are expressed in square meters and are given for a "Top" direction normal to the diametral plane and in a "Side" direction at right angles. The effective cross-section areas can be compared to the maximum geometric cross-section given in the last row of Table 1. Also noted are the number of spines necessary for any given packing fraction and spine diameter.

Figure 9 shows a plot of the effective area of the module vs. geometrical area as a function of three spine diameters (1, 1/2 and 1/4 inches) and two packing fractions (0.5 and 0.7). The effective and geometric areas corresponding to spine radii of 2, 3 and 4 meters are clearly marked on the curves.

3.5 Optical Efficiency

The design and predicted sensitivity of the Sea Urchin module have been discussed in the above sections. In order to verify the predicted performance of the detector we have carried out measurements on the quantum yield of the selected fluor, and measurements of the optical efficiencies of single spines. These are described in detail in Ref. [5].

3.5.1 Quantum Yield Measurements - - An experiment was conducted to determine the quantum yield of the two most effective fluors tested, Hostasol Yellow 8G and 3G, dissolved in toluene. In these measurements we used a spectrophotofluorimeter* of special design [6]. Measurements were taken with the fluors illuminated at the wavelength of the mercury line 436 nm. Quantum yields were measured following a procedure described by Parker [7], which compares the spectral yields of the fluors with that of a standard solution, in our case fluorescein in 0.1N NaOH. A sketch of the apparatus used in these measurements is shown in figure 10.

The results for both Hostasol Yellow 8G and 3G indicate quantum yields well above 90% with an estimated error not in excess of 10%.

3.5.2 Optical Efficiency Measurements - - In determining spine optical efficiency, the equivalent area for light collection of a single spine was measured by the arrangement shown in figure 11. In (a) the spine was exposed to the source, which is filtered to yield a spectrum simulating that of Cerenkov light underwater. The spine was optically coupled to the PMT by optical grease, and the signal measured in a manner similar to that described above in section 3.2. In (b), the PMT is exposed directly to the same illumination with a mask M that exposes a known area of PMT photocathode. Comparison of the two measurements yields the equivalent effective area of the spine, and thus the efficiency ϵ : i.e.

$$\epsilon = \text{Effective spine area/Geometrical area}$$

Note that in taking the measurements no corrections for spectral absorption efficiency, source strength, capture efficiency, PMT cathode spectral sensitivity, etc., were necessary; the measurements included all such corrections. The ratio of the equivalent spine area, thus determined, to the geometric cross-section of the spine is the optical efficiency of the spine.

Observations were recorded with both Hostasol Yellow 8G and 3G, at several different concentrations, using PMT's with S11A, S1, and S20 cathodes. Our observations on a single 8-foot one-inch diameter spine gave an equivalent area of 28 cm² for the optimum fluor filling, which corrects to 34 cm² for a 3-meter long spine, using the observed attenuation data. This corresponds to a spine efficiency of 4.5%.

4.0 DISCUSSION OF RESULTS

The data taken on spectral and attenuation measurements (figures 5 - 7) make it apparent that the best fluor for use in the Sea Urchin spines is Hostasol Yellow 8G dissolved in toluene. This is true from the standpoint of both light output and cost.

*We are indebted to Prof. R. H. Mackay for the use of his apparatus.

4.1 Attenuation Length.

The usefulness of the concept of attenuation length as applied to the fluorescent spectrum deserves some comment. Figure 6 shows that the attenuation of a single wavelength near the peak of the spectrum behaves as a single exponential; the concept of attenuation length is clearly applicable. Figure 7 shows the same fluor and solvent taken without a spectrometer, so that the attenuation measured is that of the fluorescent signal integrated over the whole spectrum. This figure shows a totally different attenuation behavior, which was discussed above in Sec. 3.3.

One can introduce the concept of incremental attenuation length, the value corresponding to the slope at any position; this is useful for evaluating the gain from extending the spine length. But it is clear that one cannot calculate the total light obtained from a spine just from a single reading and an attenuation length.

4.2 Comparison of Observed and Calculated Efficiencies.

Using the CYL6X program, it has been possible to investigate the effect of various parameters on the efficiency of the spine. In particular it has been possible to find the incremental value of an increase in the index of refraction of the solvent, the importance of parameters like the surface reflection coefficient, the attenuation coefficient of the incident light, etc. It has also been possible to search for values of the coefficients yielding results that simulate the measured values found with real spines in the laboratory.

The results of the spine efficiency measurements discussed above indicate that the observed efficiencies fall below those calculated from the CYL6X light transformation program by about a factor of two. This is believed due to the effect of fluorescence reabsorption and reemission, since the absorption and emission spectra of these fluors overlap. This effect is not taken into account in the CYL6X program. Figure 12, showing the fluorescent spectra of Hostasol Yellow 8G and 3G, excited by the 436 nm mercury line, demonstrates this phenomena. Spectra marked A are for extremely dilute solutions, in which reabsorption of fluorescent light is negligible; curves marked B are typical of spines using concentrations that yield maximum light output. The vertical scales are arbitrary and are not comparable for any two curves. The effect of the reabsorption is to cut off the short wavelength end of the fluorescent spectra; the fraction lost is of the order one-half, in rough agreement with the observed loss of efficiency.

With our observations on a single spine yielding an equivalent area of 28 cm^2 for an 8-foot spine and 34 cm^2 for a 3-meter long spine, and with the opacity program, it is possible to calculate the Sea Urchin module sensitivity. The total equivalent area of the Sea Urchin detector can be written

$$A = A_0 \times \text{OPF} \times e_0 f \times C$$

where

A_0 is the geometric area of the module: the area of a circle whose radius is the spine length plus the radius of the glass sphere;

OPF is the opacity factor, which is the ratio of the area actually oc-

cupied by the spines to the geometric area for any specific spine diameter, sphere radius, and packing fraction;

e_o is the observed efficiency of the spine, defined as the ratio of effective area of the spine to geometric cross-section;

f is a calculated factor which converts the efficiency in air to the efficiency when immersed in water;

C is the fraction of the emergent light from the spine that reaches the PMT photocathode (taken from the CYL6X program).

4.3 Specific Designs.

Two important design possibilities were considered for Sea Urchin. One used an 8-in PMT and 17" sphere, with 3-m spines. The second uses a 13" PMT and a 26" sphere, with 8-ft spines. In determining the total equivalent area A for the latter case, we have:

$$\begin{aligned} A_o &= \pi(2.44 + 0.33)m^2 = 24.1 \text{ m}^2 \\ e_o &= 28 \text{ cm}^2 / 619 \text{ cm}^2 = .045 \text{ (from section 3.4)} \\ f &= 0.48 \\ OPF &= 0.697 \text{ (the increased sphere size now allows for} \\ &\quad \text{900 one-inch spines at packing fraction 0.666)} \\ C &= 0.80 \end{aligned}$$

yielding:

$$A = 0.290 \text{ m}^2$$

The sensitivity S , defined as the number of photoelectrons delivered to the first dynode in an incident Cerenkov flux of 100 quanta/cm², becomes:

$$S = .25 \text{ (PMT cathode efficiency)} \times 100 \times A = 7.25$$

The overall Sea Urchin module diameter is 5.54 m. The above calculations for equivalent area refer to Cerenkov light normal to the Sea Urchin diametral plane. The effective equivalent area for light directed at right angles to that would be decreased in accordance with the opacity calculation data of Table 1 and Figure 9.

4.4 Cost.

The cost of Hostasol 8G is about \$75/lb, or less than \$.20/gm, and it is used in concentrations of 25-50 mgm/liter. This is far less than most other fluors used in WLS devices. The cost of toluene depends strongly on the quantity ordered as well as the purity required. We have found that the technical grade of toluene, available in 55-gallon drums (and larger containers), yields as much light as research-grade purified toluene. The impurities in technical toluene, mainly other hydrocarbons, do not adversely affect the fluorescence.

The cost of technical-grade toluene, in very large quantities, is about the same as that of gasoline; in smaller quantities it is somewhat more. Thus the cost of materials to fill an 8-ft 1-in diameter spine is well under \$.50. The glass tubes themselves are manufactured by Sylvania Glass Co.

for use as fluorescent bulbs, and are also inexpensive (although sealing their ends may not be.) Thus the overall spine cost is far lower than the usual BBQ WLS bars, implying that glass containers with toluene fluor solution fillings would make inexpensive and efficient WLS bars.

5.0 CONCLUSIONS

Sea Urchin is a highly sensitive, although fragile and complicated detector. The new Hamamatsu 20" PMT has a sensitivity of 4 in our units, two-thirds that of the Sea Urchin based on smaller PMT's. A Sea Urchin design based on the 20" PMT, with an optical gain of 5 to 10, would be feasible only if the spine length can be usefully extended beyond 3 meters.

The Sea Urchin concept also provides the optical equivalent of an electronic addition circuit.

This work was supported in part by a Department of Energy grant, under DOE Contract DE-AM03-76SF00235.

REFERENCES

- [1] W.W.Viehmann and R.L.Frost, "Thin Film Waveshifter Coatings for Fluorescent Radiation Converters," NASA Tech. Memo. 79723, 1979.
- [2] T. Bowen, "A Glass Pipe Inductively-Coupled DUMAND Photodetector Module", Proc. DUMAND 1979 Workshops at Khabarovsk and Lake Baikal, p. 13, J.G.Learned, ed. Hawaii DUMAND Center, Honolulu, HI, 1980
- [3] D. McGibney, A. Roberts and U. Camerini, "The Sea Urchin Module, I. Survey of Design Problems", Vol. 1, p.26, Proc. of DUMAND Intl.Symposium, Honolulu, 1980, V.J.Stenger, ed. (hereafter called DUMAND 1980). Hawaii DUMAND Center, Honolulu, HI., 1981.
- [4] D. McGibney and A. Roberts, "Design of the Sea Urchin Module, II. Spine Design", DUMAND 1980, Vol. 1, p. 40.
- [5] A. Roberts and D. McGibney, "Design of the Sea Urchin Module, III. Experimental Measurements of Spine Efficiency, and Redesign for Improved Sensitivity", DUMAND 1980, Vol. 1, p. 59.
- [6] R.H. Mackay, Arch. Biochem. Biophys., 135, 218 (1969).
- [7] C.A. Parker, Photoluminescence of Solutions, Sec. 3L; Elsevier, London, 1968.

Figure Captions.

Fig. 1. Drawing of Sea Urchin, showing the spines radiating from the surface of the hemisphere containing a hemispherical-cathode PMT. The lower glass hemisphere has been removed to show the PMT.

Fig. 2. The geometry of Sea Urchin. The radius of the PMT is so chosen that all (or most) of the light emitted by each spine strikes the photocathode, ensuring a good phase-space match. To minimize losses, the space between the glass hemisphere (spherical lens) and the PMT should be filled by a transparent medium with the same index of refraction.

Fig. 3. Construction of light box used to illuminate sample spines with simulated Cerenkov light.

Fig. 4. Experimental apparatus for measurement of fluorescent spectrum.

Fig. 5. Emission spectra of selected fluorescent dyes in solution. Curves are to the same scale, and can be compared.

Fig. 6. Attenuation of fluorescent radiation, using apparatus of Fig. 4. Measurements are at a single wavelength at the peak of the fluorescent spectrum. They are differential; they show the light intensity from a fixed length L as a function of distance from the spectrometer. Fluor is Hostasol 8G; spine is $1/2$ " diam.

Fig. 7. Same conditions as Fig. 6, but taken without the spectrometer. The entire spectrum is observed at once. Note the great deviations from exponential attenuation.

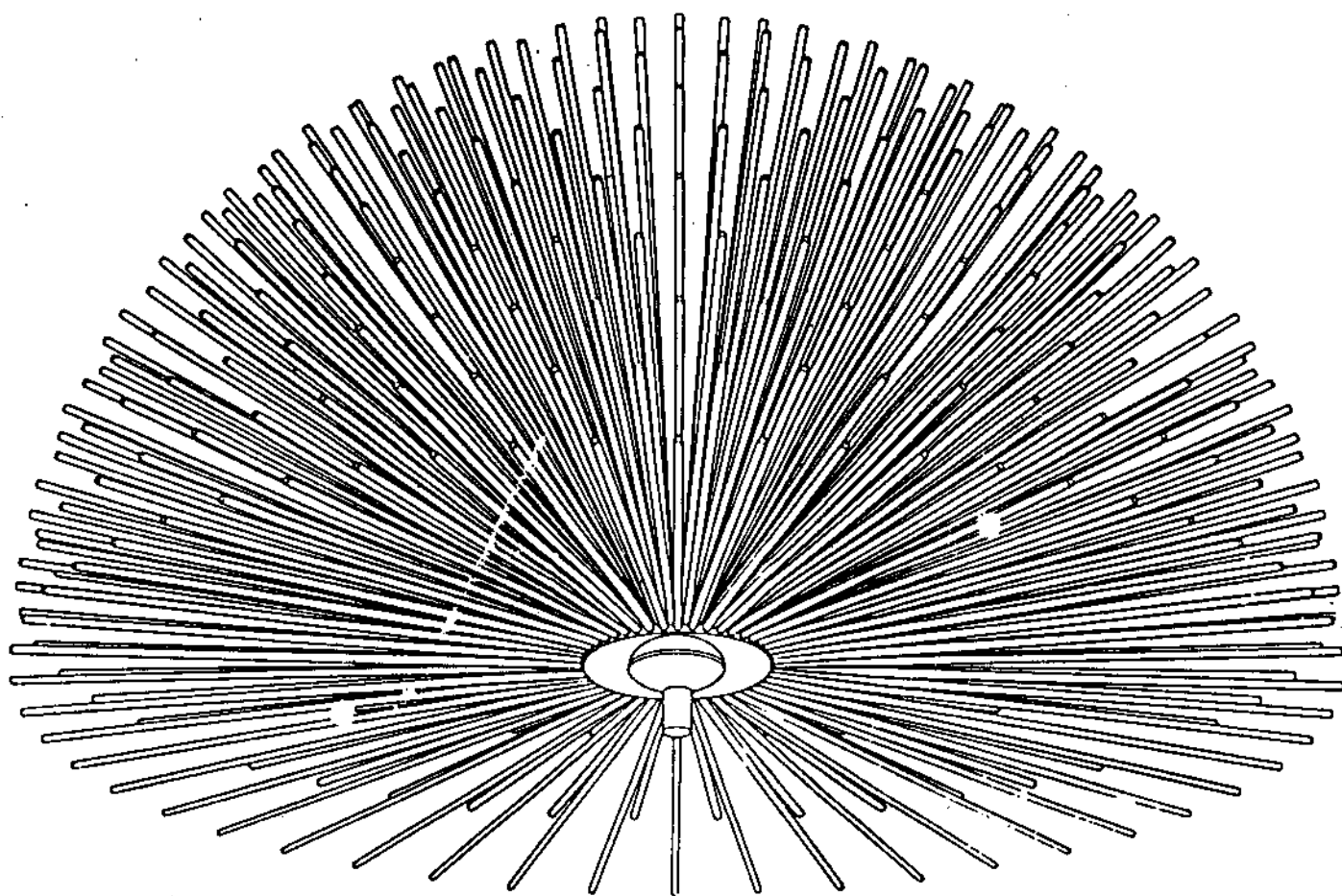
Fig. 8. a). Predicted angular distribution of light reaching the end of the spine, for very low attenuation, variable surface reflection. b). Same, for a moderate value of attenuation. Note how cone narrows with increasing attenuation.

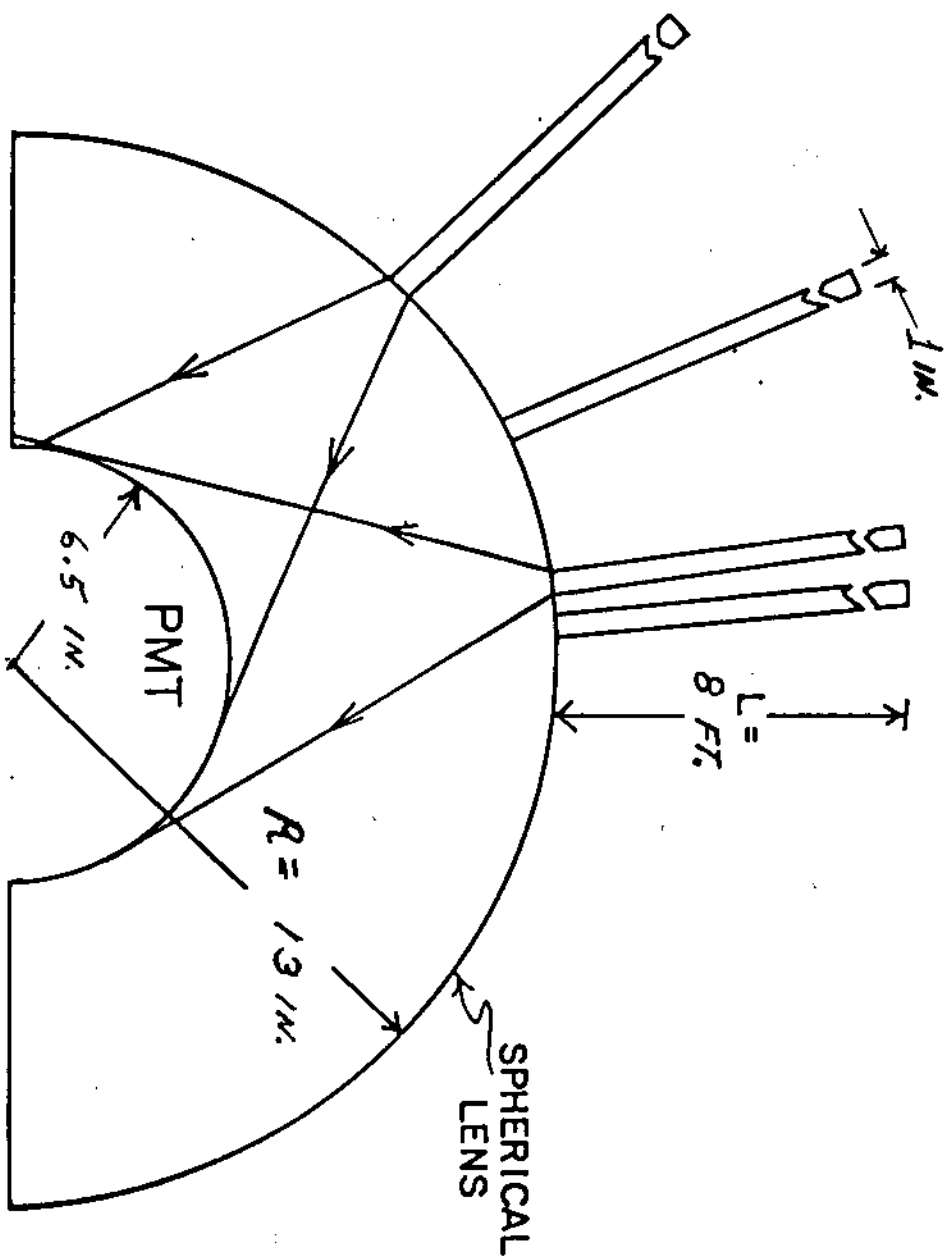
Fig. 9. Effective area of a Sea Urchin detector vs. geometrical area, as a function of spine diameter and packing fraction (P.F.), the fraction of the glass area of the sphere occupied by spines. Areas corresponding to spine radii of 2, 3, and 4m are indicated.

Fig. 10. Spectrophotofluorimeter arrangement for measuring the quantum yield of fluors, by comparison with a standard.

Fig. 11. Apparatus for measuring the effective area of a fluorescent spine. a). Arrangement for reading spine output with PMT. b). Arrangement for observing PMT response directly. The mask defines the photocathode area. The ratio of the readings determines the effective area of the spine.

Fig. 12. Fluorescence curves for Hostasol 8G and 3G, for very dilute solutions (curves marked A) and solutions of maximum light yield (curves marked B). The difference is due to reabsorption of the blue end of the fluorescent spectrum, and re-emission at longer wavelengths.





SEA URCHIN

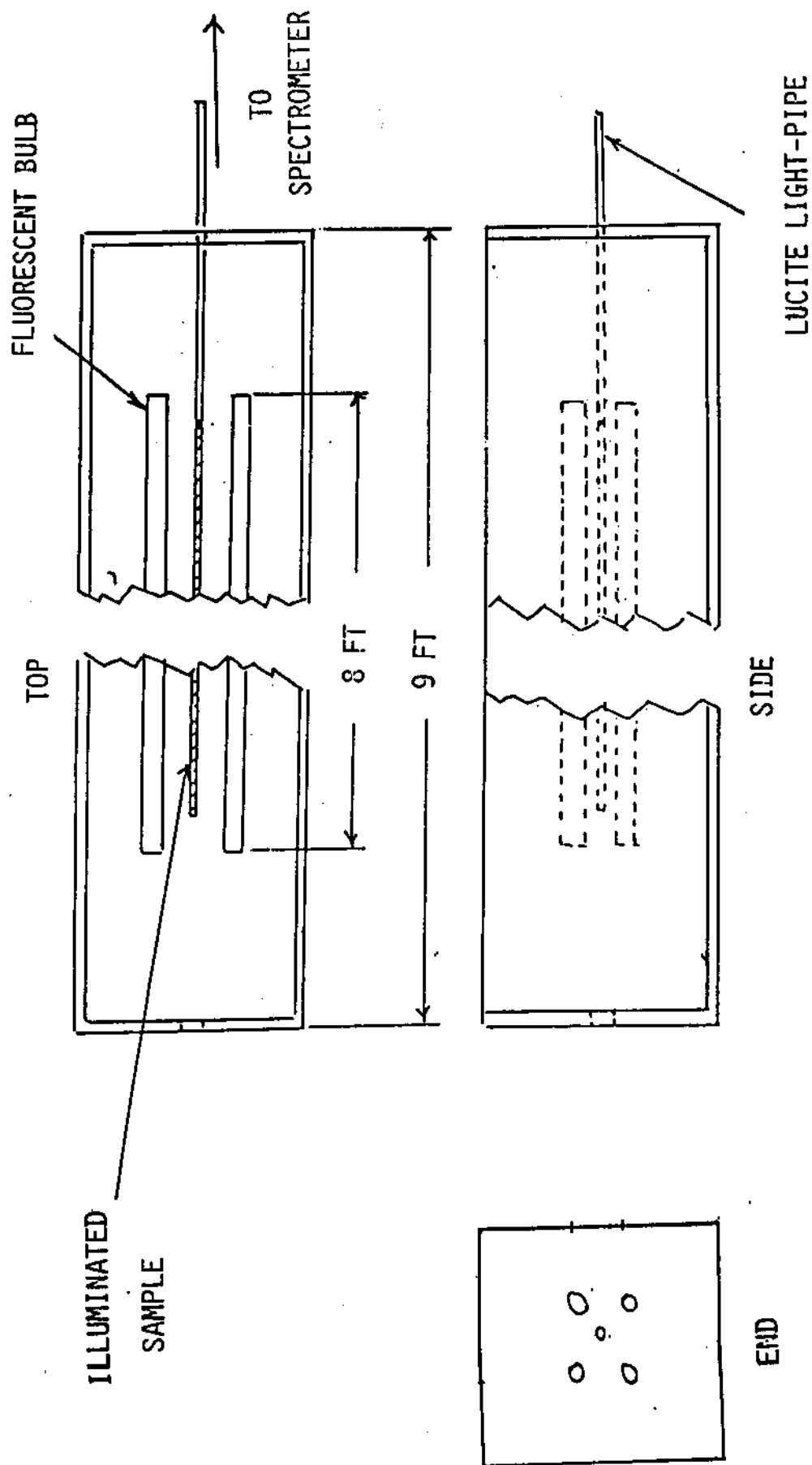
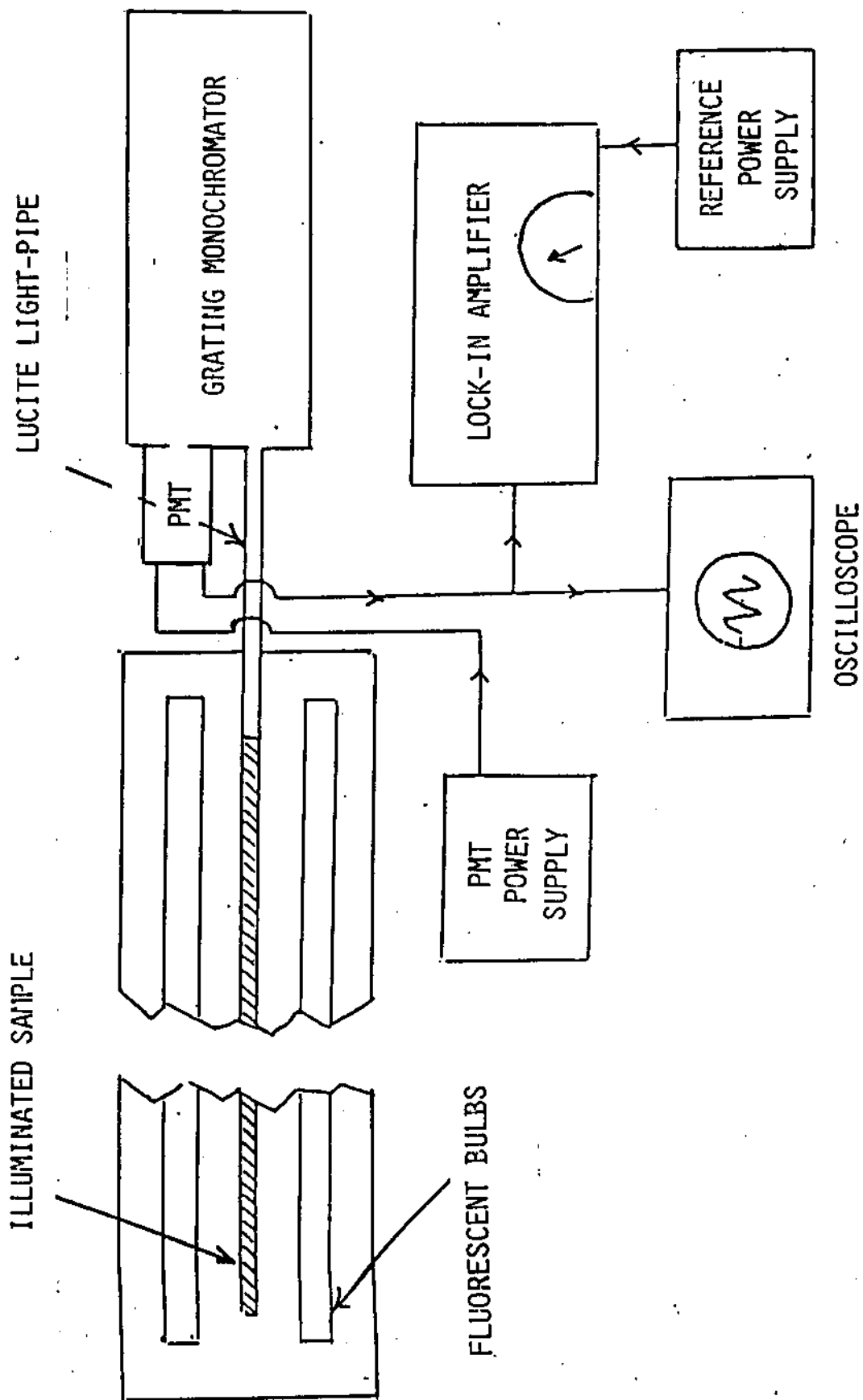


Fig 4



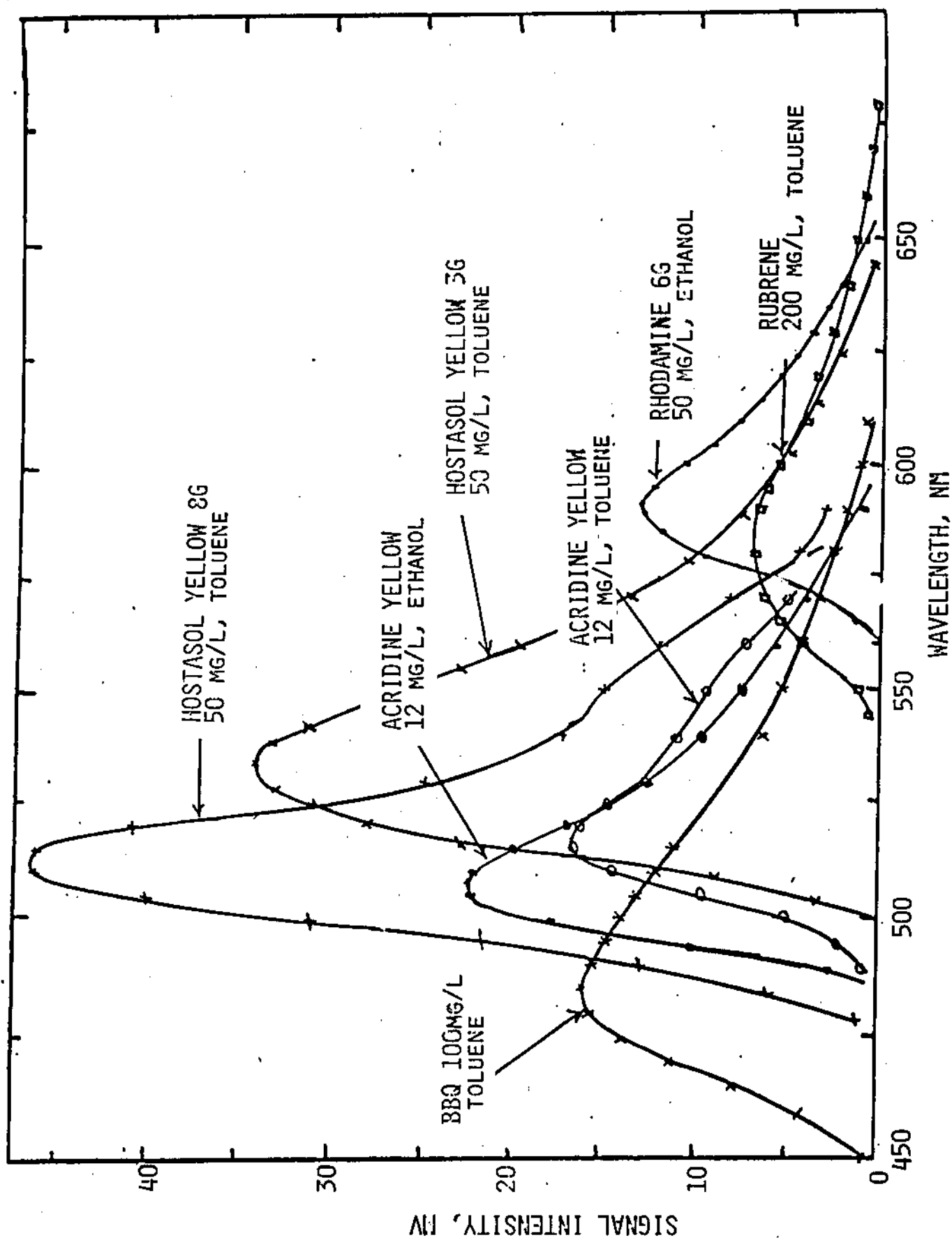
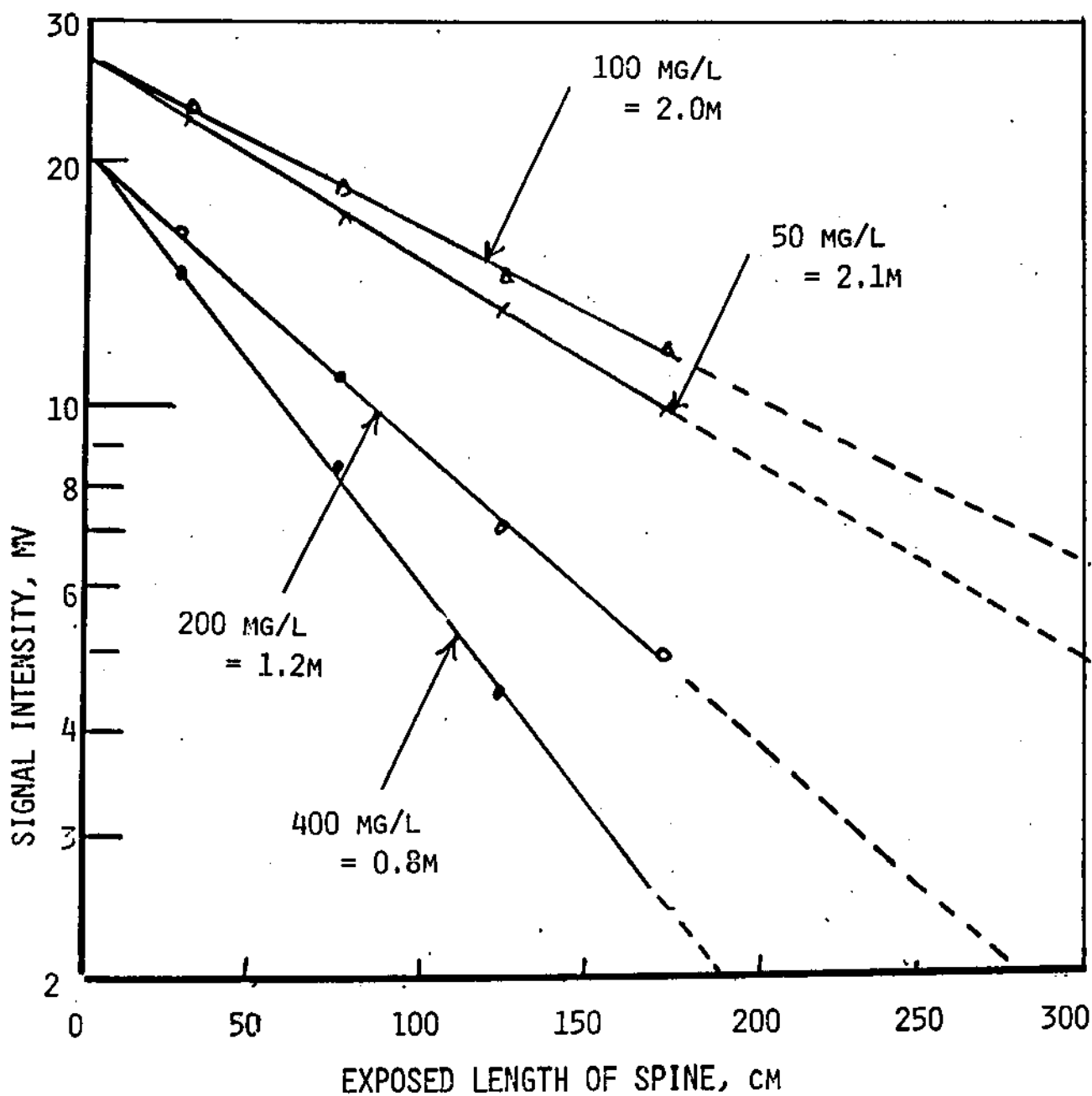
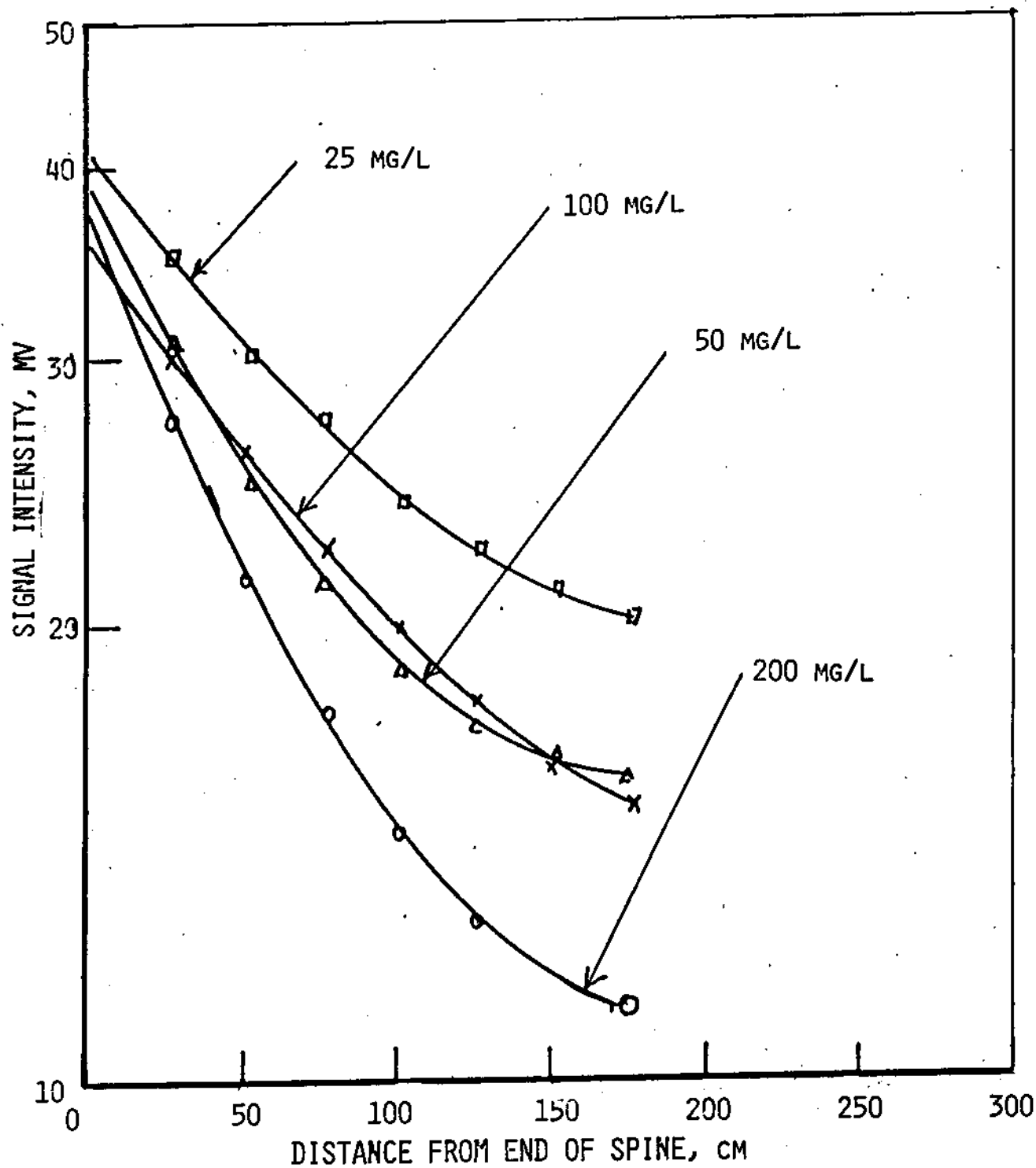
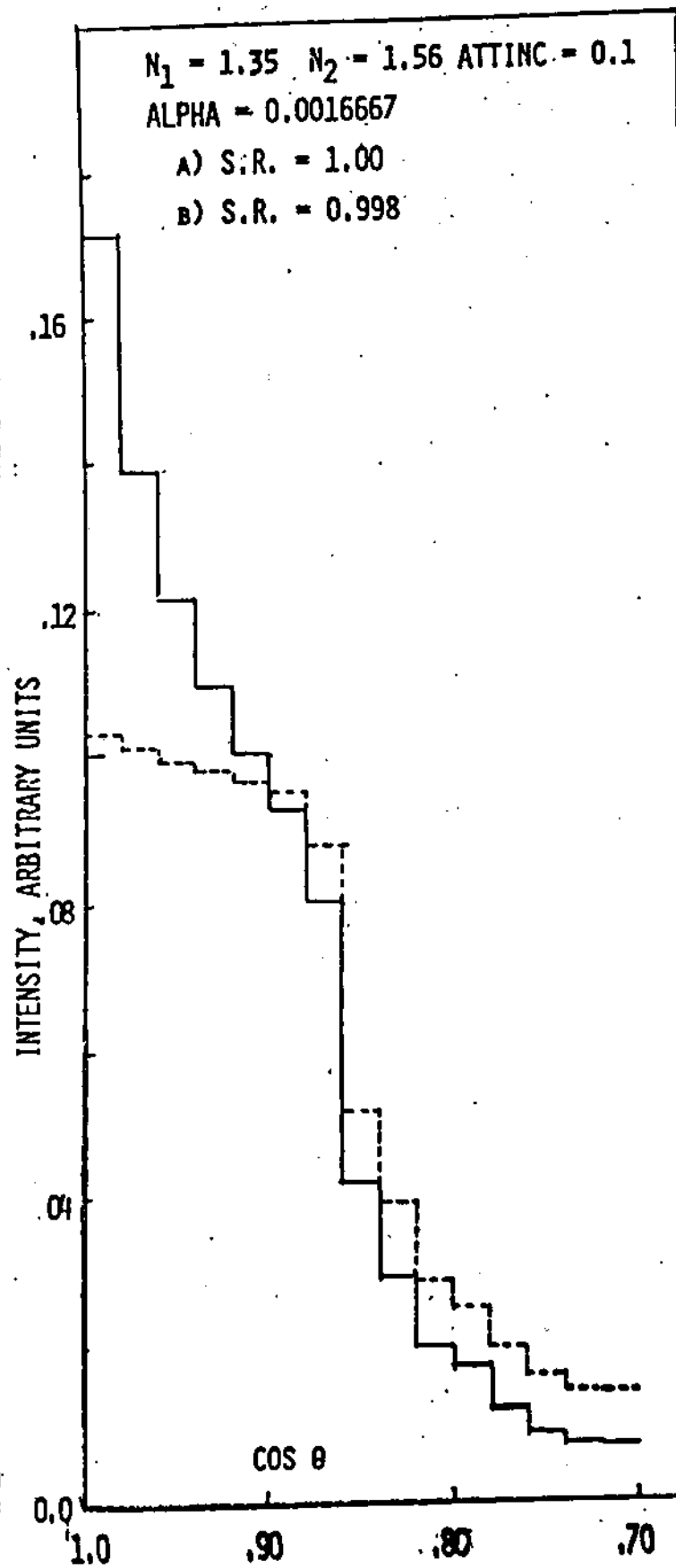
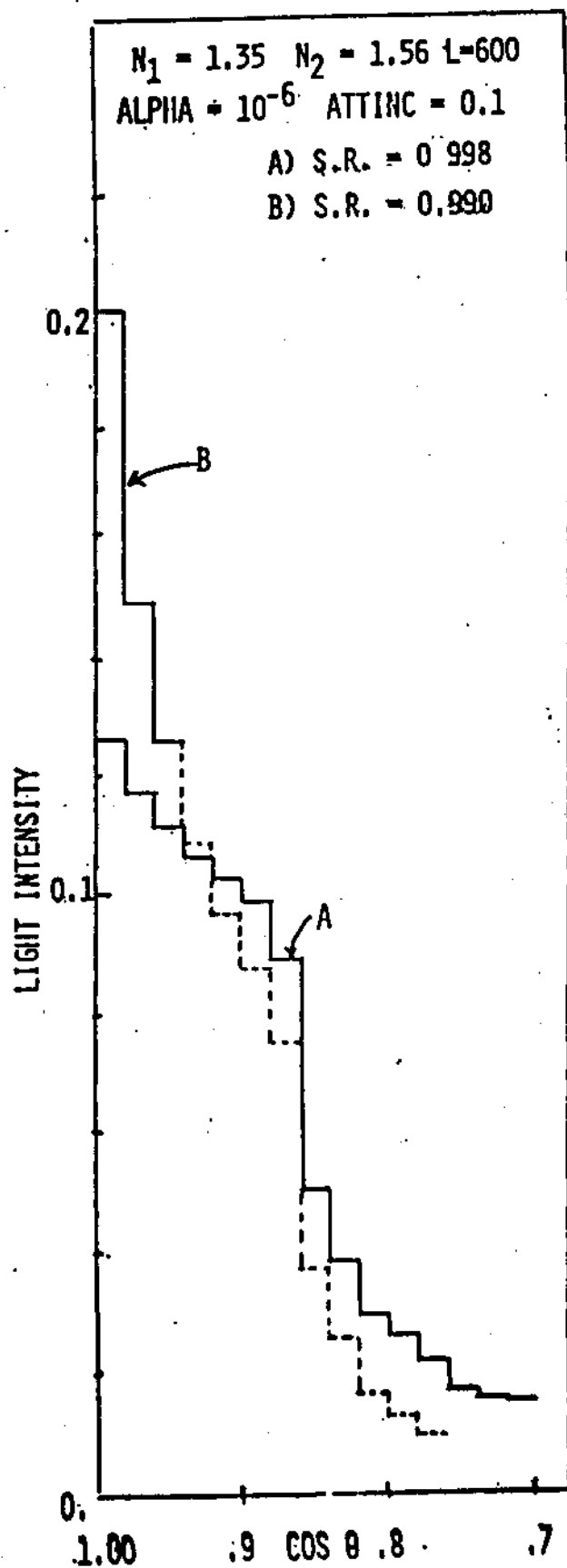
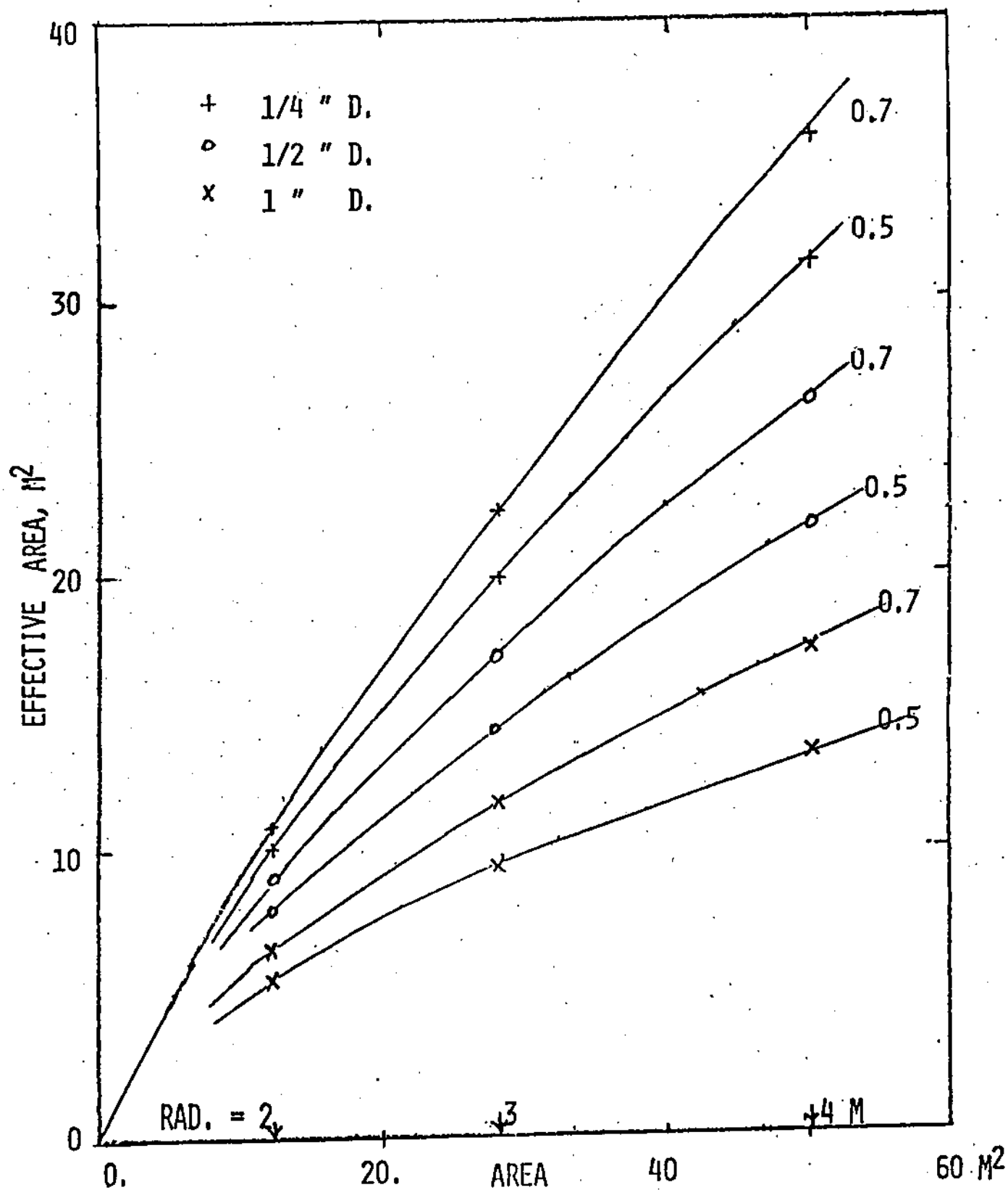


Fig 6









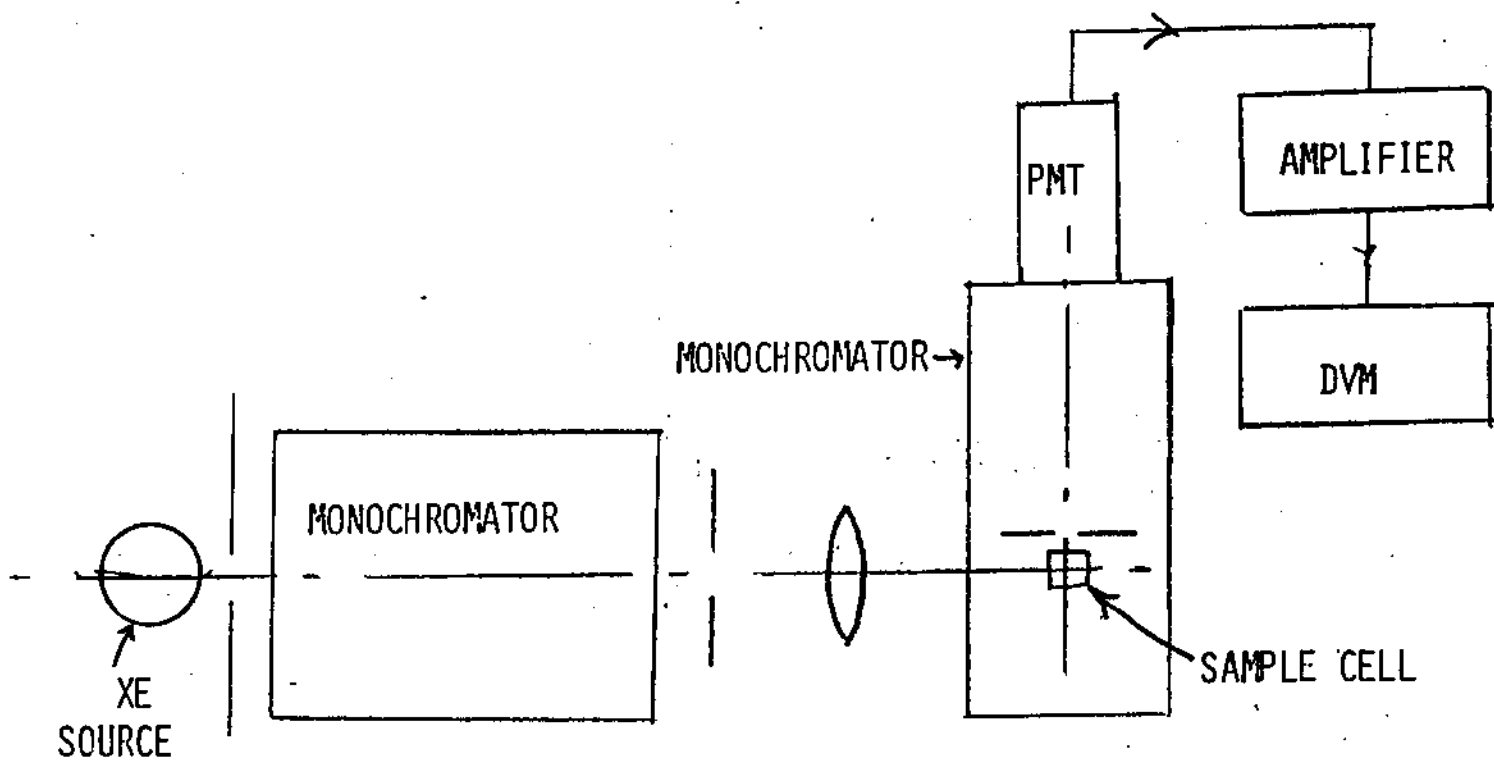
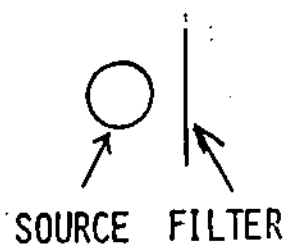
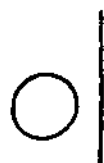


Fig 10



(a)



(b)

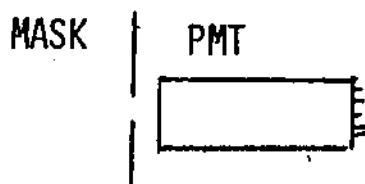
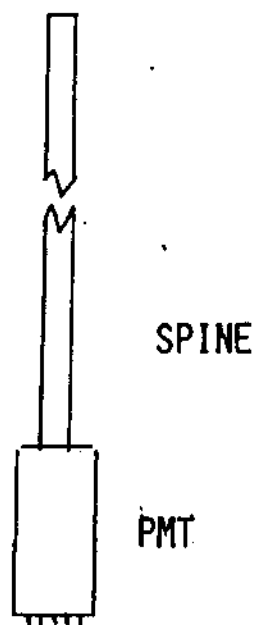


Fig 11

INTENSITY, ARBITRARY UNITS

